crystals

MDPI

Article

Dielectric Response of ZnTe–Ti/Al Schottky Junctions with CdTe Quantum Dots Studied by Impedance Spectroscopy

Eunika Zielony [1,*], Ewa Płaczek-Popko [1] and Grzegorz Karczewski [2]

[1] Department of Quantum Technologies, Wroclaw University of Science and Technology, Wybrzeze Wyspianskiego 27, 50-370 Wroclaw, Poland; ewa.popko@pwr.edu.pl

[2] Institute of Physics, Polish Academy of Sciences, al. Lotnikow 32/46, 02-668 Warsaw, Poland; karcz@ifpan.edu.pl

* Correspondence: eunika.zielony@pwr.edu.pl; Tel.: +48-71-320-26-42

Received: 6 February 2020; Accepted: 4 March 2020; Published: 6 March 2020



Abstract: The electrical properties of ZnTe–Ti/Al Schottky junctions were investigated by the impedance spectroscopy (IS) method. Current-voltage (*I-V*) and capacitance-voltage (*C-V*) measurements were also performed. The studied samples were the CdTe quantum dot structures embedded in ZnTe matrix and a reference ZnTe sample without quantum dots. *C-V* characteristics confirmed the presence of quantum dots (QDs) in the structures. Electric modulus and impedance data were analyzed. IS studies proved that long-range conductivity governs the relaxation processes in the junctions. For both samples, the data were fitted with a simple *RC* circuit composed of a depletion layer capacitance in parallel with bulk resistance and a series resistance of contacts. The activation energy of the relaxation process observed for the reference sample obtained from the Arrhenius plot of the resistance, imaginary impedance, and electric modulus equals 0.4 eV at zero bias. For the quantum dot sample, the value of activation energy determined with the help of the same methods equals 0.2 eV. In conclusion, it was assumed that the relaxation processes for the reference sample are attributed to the trap present in ZnTe host material, whereas those observed for the QD structure are assigned to the deep level associated with defects located close to the QDs created during their growth.

Keywords: ZnTe; CdTe; quantum dots; defects; impedance spectroscopy

1. Introduction

Self-organized quantum dots (QDs) have been investigated widely for several years for comprehension of fundamental physics of zero-dimensional structures and for their attractive application in QD semiconducting devices, such as lasers, detectors of radiation, or solar cells. The most important parameter determining the thermal emission of carriers from the dots is the energy level position of discrete QD states relative to the band edges of the barrier material [1]. Quantum dot layers embedded in a semiconducting structure behave like giant traps, and thus the techniques used to study deep traps in standard semiconductor devices became applicable for QD structures. Deep level transient spectroscopy (DLTS) is a widely used technique to study the parameters of deep traps present in the energy gap of semiconductor junctions [2]. Besides the DLTS method, impedance spectroscopy (IS) has become the most common technique to probe electronic properties of QD systems [3]. It is an alternating current (AC) electric technique used to observe the current response of a system to which an AC voltage is applied as a function of the frequency. The impedance spectroscopy (IS) measurement enables the investigation of electric properties of a bulk and an interface that we cannot study by standard direct current methods because the electric response speed of each component is

different on the microscopic time scale [4]. The measurement principle in the IS relies on the excitations of electrons captured by deep traps present in the depletion region of the junction by changing its polarization conditions. Therefore, IS gives insight into carrier kinetics in a way similar to the DLTS technique. Moreover, IS is a technique that is used for the identification of relaxation processes that determine the electric response of a device.

Zinc telluride (ZnTe) with a direct band gap of 2.26 eV at room temperature [5] and low electron affinity of 3.53 eV [6] has found many applications in optoelectronics and integrated optics. Quantum dots are still of wide interest because of their highly tunable properties that change with their size and shape [7]. II-VI QDs also belong to the diverse family of QD systems. Among them, CdTe QDs embedded in ZnTe matrix are an interesting alternative for the direct excitonic transition with the spectral range corresponding to green light. Taking into account a wide range of applications of QDs, there is still a continuous need for basic research of these nanostructures, in the form of various semiconductor compounds.

CdTe/ZnTe QD systems grown by molecular beam epitaxy have been examined by other authors, mainly by optical measurement techniques, such as photoluminescence [8–10]. This is because of well-known technological problems concerning obtaining efficient Schottky or *p*-*n* junctions based on CdTe and ZnTe compounds [11,12], which are necessary to perform electrical measurements. Nevertheless, recent articles on CdTe/ZnTe quantum dots show that research on this QD system is still conducted [13–15]. However, impedance spectroscopy measurements of CdTe/ZnTe QD Schottky junctions have not been reported by any authors so far. To the best of our knowledge, the IS method has been applied in the case of other QD systems, such as InAs/GaAs [16], $CuGaS_2$ [17], or PbS [18,19].

In this work, current-voltage (*I*-*V*) and capacitance-voltage (*C*-*V*) measurements as well as the impedance spectroscopy technique were applied to investigate ZnTe (*p*-type)–Ti/Al Schottky diodes containing a layer of CdTe self-assembled quantum dots. In order to distinguish the IS signal related to quantum dots, two types of samples with the same layer structure were studied: a reference sample without quantum dots and a sample grown at the same conditions containing an assembly of CdTe quantum dots. *I*-*V* measurements were used to study the rectifying properties of the diodes, while the *C*-*V* method was applied to determine the concentrations of carriers. On the basis of impedance spectroscopic measurements, the activation energies of the traps in both samples were calculated and compared. Additionally, an equivalent *RC* circuit model was proposed for the investigated Schottky junctions. The obtained results helped us to understand the principle of operation as well as mechanisms of charge transport in the investigated Schottky junctions. Moreover, they provided information on defects in the studied samples as well as on the influence of quantum dots on their electrical properties.

2. Materials and Methods

Two types of samples with the same layer structure were analyzed: a reference sample without quantum dots and a sample with self-assembled quantum dots. All samples were grown by molecular beam epitaxy. The latter sample consists of 3 µm thick p^+-type ZnTe/N buffer deposited on the *p*-type GaAs substrate, 0.6 µm *p*-type ZnTe/N, the layer of CdTe QDs, and 0.11 µm of *p*-type ZnTe/N cap. The CdTe QDs formed spontaneously as a result of the deposition of three monolayers of CdTe embedded in ZnTe matrix. The presence of QDs was confirmed by photoluminescence measurements run at 10 K (cf. [12]). More technological details about the samples can be found in our previous paper [12].

The AuZnAu ohmic contacts were formed on the GaAs substrate layer and Schottky Ti(5 nm)/Al(200 nm) contacts were deposited by the photolithography on the cap ZnTe/N layer. The IS measurements were performed using a Novocontrol impedance analyzer (Novocotrol Technologies GmbH & Co. KG, Montabaur, Germany). The obtained data were analyzed with the help of a Solartron Z-plot software. Each measurement was done applying a 20 mV alternating current (AC) sinusoidal

signal over the constant applied bias. The impedance measurements were performed in the frequency range from 0.1 Hz to 3 MHz, at temperatures from 77 to 300 K.

3. Results and Discussion

3.1. I-V and C-V Measurements

Electrical measurements of current-voltage (*I-V*) characteristics were realized to check the rectifying properties of the investigated diodes. A standard equation describes the current I through a Schottky junction [20]:

$$I = I_S\left\{exp\left[\frac{q(V - IR_S)}{nk_BT}\right] - 1\right\} \quad (1)$$

where I_S is the saturation current, q is the elementary charge, R_S is the series resistance, T is the temperature, n is the ideality factor, and k_B is the Boltzmann constant. The saturation current is given by the following formula [20]:

$$I_S = SA^*T^2exp\left(\frac{-q\Phi_B}{k_BT}\right) \quad (2)$$

where S is the Schottky contact area, A^* is the effective Richardson constant (of 72 A/cm^2/K^2 for p-type ZnTe), and $q\Phi_B$ is the barrier height.

Figure 1 shows the *I-V* plots for the reference and QD samples, obtained at room temperature. From the linear slope of $ln\ (I) = f\ (V)$, characteristics in the forward direction barrier heights were calculated for the reference and QD samples. Their values are $q\Phi_B = 0.68\ eV$ for the reference sample and $q\Phi_B = 0.69\ eV$ for the QD sample. On the basis of the current-voltage measurements, it can be concluded that both junctions reveal rectifying properties, confirmed by the forward-to-reverse current ratio at an applied voltage of ±2 V, which equals 1.5×10^3 and 4.6×10^2 for the QD and reference sample, respectively. Moreover, the *I-V* measurements show that the presence of CdTe quantum dots in the Ti/Al–ZnTe Schottky diode does not change significantly its electric parameters.

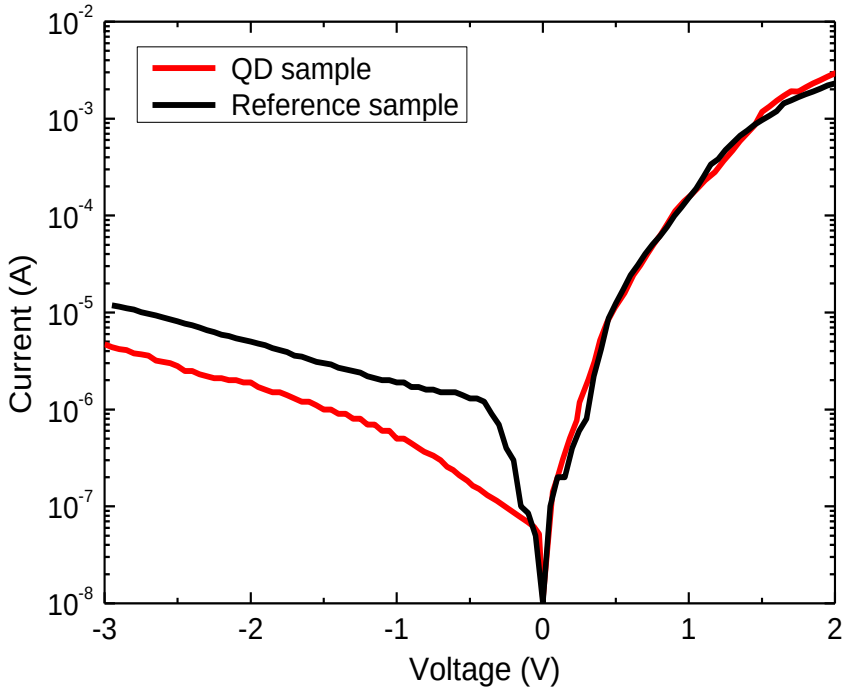


Figure 1. Current-voltage (*I-V*) characteristics of a reference- and quantum dot (QD) Ti/Al–ZnTe Schottky diode.

In the *C-V* measurements, an AC signal of 1 MHz frequency is superimposed on the direct current (DC) reverse bias. The AC signal modulates the charge at the edge of the depletion layer width and at the point where the Fermi level crosses the quantized levels in QDs. Thus, the capacitance of the structure with quantum dots consists of two parts [21]:

$$C = C_{3D} + C_{QD} = \frac{dQ_{3D}}{dV} + \frac{dQ_{QD}\left(E_{QD} - E_F\right)}{dV} \tag{3}$$

where C_{3D} is the bulk capacitance, C_{QD} is the component of the capacitance associated with the quantum dot layer, and E_{QD} is the position of the carrier level in the quantum dot with respect to the Fermi level (E_F) in the host material. If the capacitance of QDs' predominates, the *C-V* plot exhibits a characteristic step related to the accumulation of carriers in the QD states. If the bulk capacitance is much bigger than that related to QDs, the *C-V* plot exhibits ordinary bulk behavior with a reverse bias V_R: $C \sim V_R^{-1/2}$.

The depletion layer width (x_d) for a *p*-type Schottky diode polarized in the reverse direction can be calculated from the *C-V* measurements, using a standard formula [20]:

$$x_d = \frac{\varepsilon_0 \varepsilon_S S}{C} \tag{4}$$

Equation (4) can be rewritten to the expression described by Equation (5):

$$x_d = \sqrt{\frac{2\varepsilon_0 \varepsilon_S}{qN_A}(V_{bi} + V_R)} \tag{5}$$

where ε_S is the semiconductor permittivity, ε_0 is the permittivity in vacuum, V_{bi} is the built-in potential of the metal-semiconductor junction, and N_A is the net acceptor concentration. On the basis of Equation (5), the net acceptor concentration can be estimated, if the value of V_{bi} is known.

The *C-V* characteristics of both junctions measured at room temperature are shown in Figure 2. From the *C-V* plots, on the basis of Equation (5), the net acceptor concentrations for both samples were estimated. They are in the order of 10^{15} cm^{-3}. The values of V_{bi}, calculated from the *C-V* measurements, are V_{bi} = *1.1 V* for the reference sample and V_{bi} = *0.5 V* for the QD sample. The reference sample exhibits smooth characteristics, typical for bulk semiconductor-metal junction. A characteristic step ("plateau"), which is normally seen within the negative voltage bias range in the *C-V* plots of samples containing quantum dots [7], appears within a positive voltage bias range of ~0.25 V to 1 V in the case of the investigated QD sample (cf. Figure 2). The step informs about charge accumulation on discrete states of CdTe quantum dots. Filling of quantum dot energy levels with charge carriers depends on the polarization voltage applied to the junction. Along with the polarization voltage changes, the position of the Fermi level within the depletion region also changes. This in turn causes the emission of carriers—in our case, holes—from the CdTe QD levels located above the Fermi level to the ZnTe valence band. Figure 2 shows that, for negative voltages greater than 0 V, all quantum dots are empty and the junction's capacitance decreases monotonically with the increasing reverse voltage bias. Filling of quantum dots occurs for a forward bias up to 1 V. The presence of the step for the forward bias can be explained by comparison of the junction depletion region width with the distance of the CdTe QD layer from the junction surface. Quantum dots are located at a distance of 0.11 µm from the junction surface. The junction depletion layer width at zero voltage bias, estimated from Equation (5), equals ~0.2 µm. The latter indicates that, at 0 V bias, QDs are outside the edge of the depletion region. Application of a reverse bias extends the depletion layer width, which results in the shift of the depletion edge away from the layer of quantum dots. At a forward bias, the depletion layer width shortens, and at a relevant voltage, the probing of the QD layer takes place. This leads to the filling of QDs with the charge carriers, which manifests as a characteristic step on the *C-V* characteristic. Thus, the *C-V* curve shown in Figure 2 confirms the presence of QDs in the investigated

sample. Furthermore, with reference to Equation (3), it may be assumed that, in the case of a QD sample, the bulk capacitance is lower than that related to QDs.

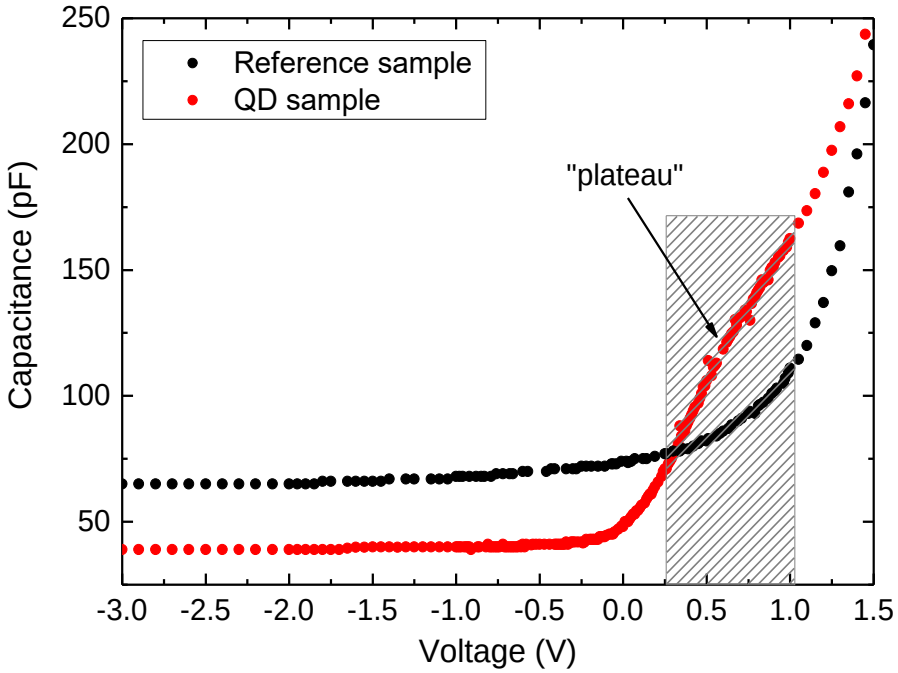


Figure 2. Capacitance-voltage (*C*-*V*) characteristics taken at 300 K for the QD (red circles) and reference samples (black circles).

3.2. IS Results

In the impedance spectroscopy (IS), standard electrical quantities such as AC voltage and AC current are measured and relevant frequency dependent properties of a material are determined. These are as follows: complex permittivity (ε^*) or dielectric constant (k^*), complex impedance (Z^*), complex electric modulus (M^*), and dielectric loss or dissipation factor ($tan\delta$). In the case of a single relaxation process, a semicircle is obtained for all the aforementioned functions when their real and imaginary parts are plotted in the complex plane. However, as shown in [22], observation of a full, partial, or no semicircle within the experimentally available frequencies depends on the relaxation ratio $r = \frac{\varepsilon_s}{\varepsilon_\infty} = \frac{C_s}{C_\infty}$, where ε_s is the real permittivity when the angular frequency ω ($\omega = 2\pi f$) approaches zero, ε_∞ is the real permittivity when ω approaches infinity, C_s is the static capacitance of the sample, and C_∞ is the frequency-independent capacitance when ω approaches infinity. Moreover, the relaxation ratio r determines the frequency corresponding to the maximum of the imaginary part of a particular dielectric function [22]. In particular, it was proved that, for a large value of r (a few hundreds), solely impedance and modulus exhibit the semicircles in a complex plane and peaks for the imaginary parts. Moreover, the peaks of imaginary modulus and impedance overlap. On the other hand, for small r (less than 10), the imaginary part of permittivity exhibits a maximum and the permittivity plotted in a complex plane shows a semicircle. The relaxation ratio r is directly related to the type of relaxation; a small value of the ratio is the result of localized relaxation, whereas long-range conductivity results in a large value of r [22].

In Figure 3a,b, real (C') and imaginary (C'') parts of capacitance versus frequency curves taken at room temperature are given. On the basis of the $C' = f(f)$ dependence (Figure 3a), the value of the relaxation ratio $r > 100$ is estimated for both samples. Moreover, the imaginary part of capacitance $C'' = f(f)$ does not exhibit any maximum within the measured frequency range. On the other hand, relaxation peaks exhibit dependences of imaginary parts of impedance (Z'') and electric modulus (M'') versus frequency, as presented in Figures 4 and 5. Therefore, we focus further analysis on these functions.

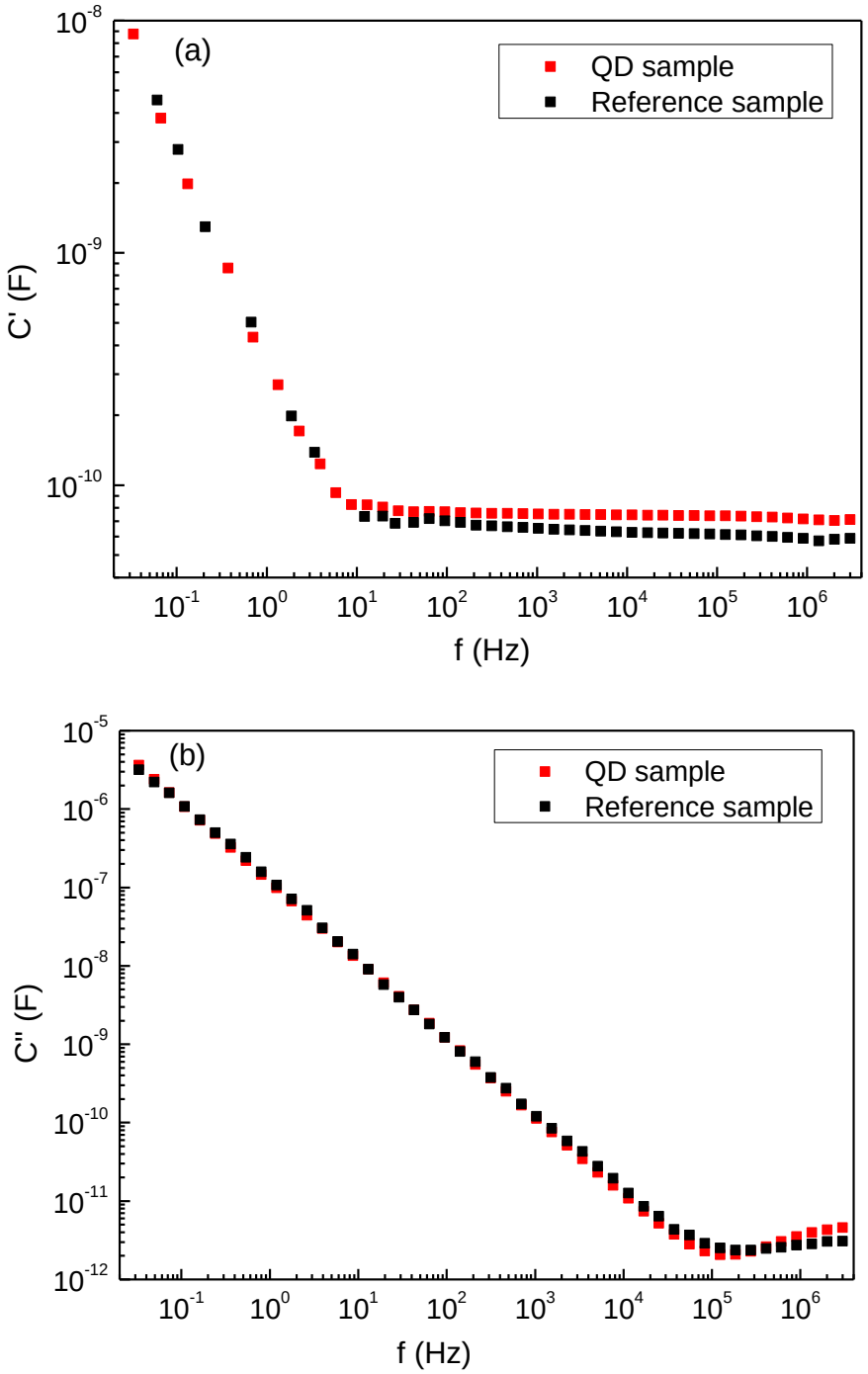


Figure 3. Double-logarithmic plots of real (**a**) and imaginary (**b**) parts of capacitance vs. frequency taken at room temperatures for the quantum dot and reference samples.

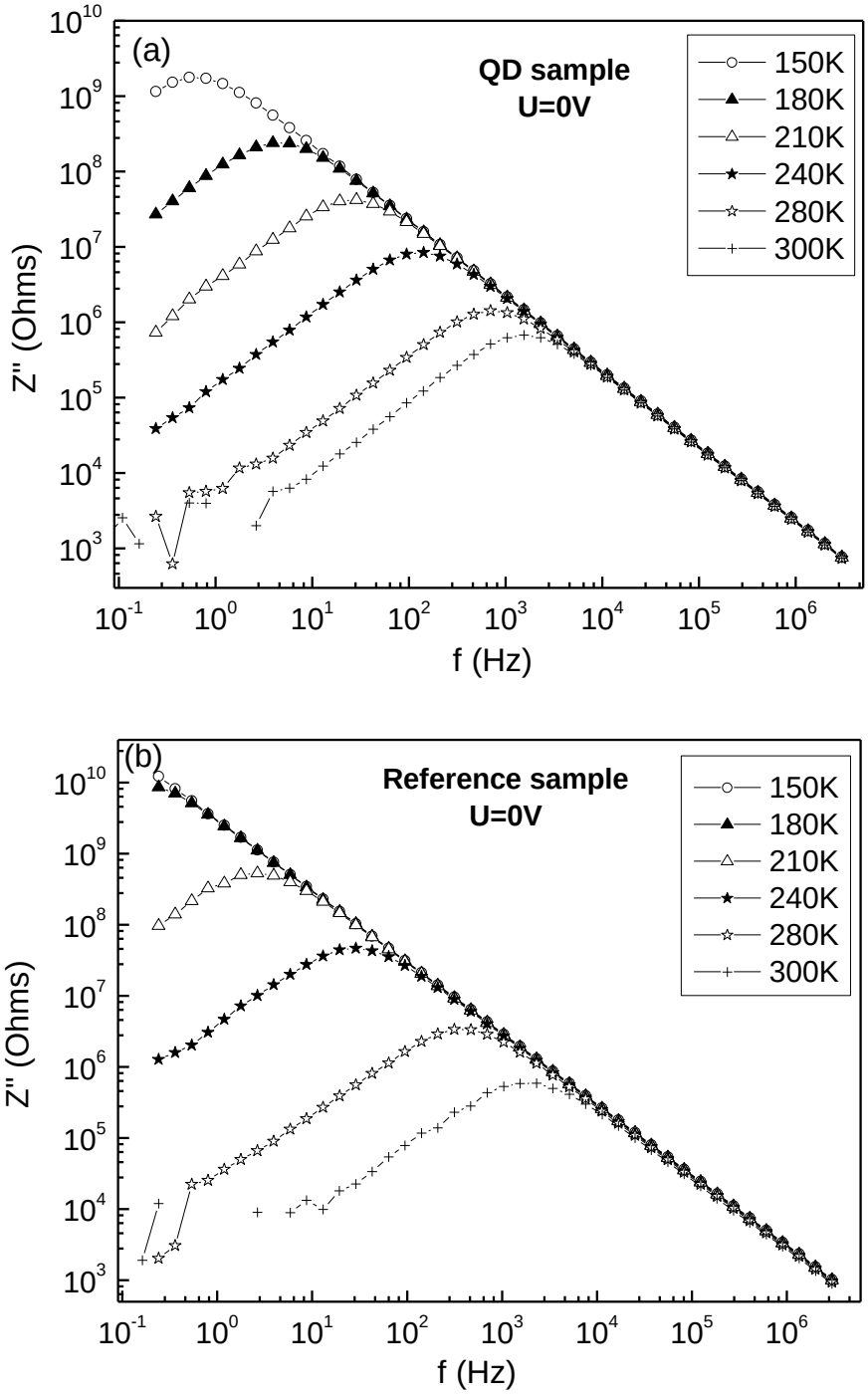


Figure 4. Double-logarithmic imaginary impedance versus frequency plots taken at different temperatures for the quantum dot (**a**) and reference samples (**b**).

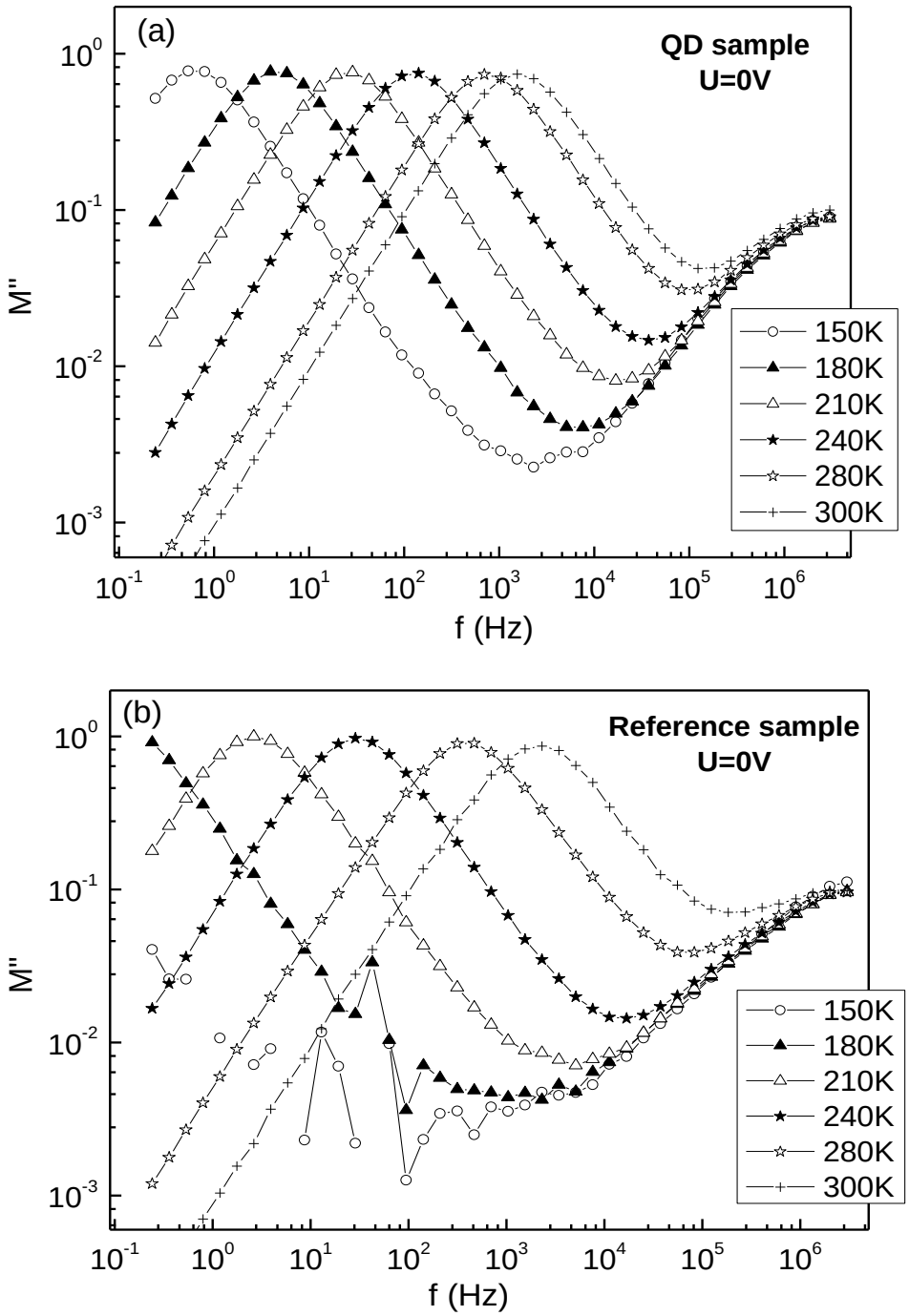


Figure 5. Double-logarithmic imaginary part of electric modulus vs. frequency plots measured at different temperatures for the quantum dot (**a**) and reference samples (**b**).

In order to understand the electric response of a studied junction, it is important to find a proper model of an equivalent *RC* circuit that represents its real electric parameters [4]. In the case of a simple parallel *RC* circuit, there is a correlation between complex impedance and electric modulus [4]:

$$M' + jM'' = j\omega C_0 Z^* = j\omega C_0 (Z' - jZ'') = \omega C_0 Z'' + j\omega C_0 Z' \quad (6)$$

where M' and Z' are the real parts of electric modulus and impedance, respectively; Z'' and M'' are the imaginary parts of electric modulus and impedance, respectively; C_0 is the vacuum capacitance of the sample holder; and $j = \sqrt{(-1)}$. A double logarithmic plot of Z'' and M'' in the frequency domain

presents a single peak, which indicates a Debye type of response [4]. Moreover, the peaks on the spectra of Z'' or M'' appear at the same relaxation frequency. The relaxation frequency (f_{max}) of the material, independently of the geometrical parameter of the sample, fulfills the following condition [23]:

$$2\pi f_{max} = \omega_{max} = \frac{1}{RC} = \tau^{-1} \quad (7)$$

If the relaxation process is thermally activated, the time constant (τ) shows an Arrhenius behavior. Thus, ω_{max} exhibits a strong temperature dependence, resulting in the peak frequency f_{max} shifting with temperature. The Arrhenius plot of τ yields its activation energy, E_a [23]. The temperature dependence of the relaxation frequency, $ln(f_{max})$ versus $1/T$, follows the same Arrhenius law (same activation energy) as τ [23].

In the case of a pure Debye type of response, the impedance and modulus complex plane plots present a single semicircle [4,24] from which the values of R (C) can be obtained. Thus, the activation energy can be also determined from the Arrhenius plot of $ln(R)$ versus $1/T$ dependence [24].

In Figure 4a,b, the plots of the zero-bias imaginary impedance Z'' versus the frequency of the probing AC voltage at different temperatures for the QD and the reference samples are shown. The impedance exhibits a single peak of amplitude decreasing with the increasing temperature and simultaneously shifting toward higher frequencies in both cases. Such behavior can be understood if one assumes that the amplitude of the maximum follows the resistance of the parallel RC circuit ($Z'' \sim R$) [4].

In Figure 5a,b, similar plots of the zero-bias imaginary part of electric modulus M'' are given for the two types of samples. In both cases, M'' exhibits a double maximum in the studied frequency range. Amplitudes of the maxima observed at higher frequency range are different and do not show any temperature dependence. It can be noted that the major peaks observed at a lower frequency range, and of higher amplitude, shift significantly toward higher frequencies with the increasing temperature. If one assumes that the amplitude of the imaginary part of electric modulus scales with the capacitance of the parallel RC circuit ($M'' \sim C^{-1}$) [4], the capacitance related to each of the relaxation peaks hardly varies with temperature. The high frequency modulus relaxation peak has not been analyzed. In order to find an activation energy related to this peak, impedance measurements at temperatures lower than 77 K have to be performed. For now, this is beyond the scope of the experiment.

In Figure 6, the imaginary part of electric modulus and impedance versus frequency plots for the QD sample (Figure 6a) and the sample without dots (Figure 6b) are shown for different temperatures. For both samples, the maxima correspond to the same frequency independent of temperature, indicating Debye-like relaxation.

In Figure 7, complex impedance plane plots are depicted for both samples at different temperatures. The plots form semicircles indicating an almost perfect Debye type of response. The dots and squares represent the experimental data, whereas solid lines stand for the fittings with a simple RC circuit shown in the inset. A typical equivalent circuit model of investigated Schottky junctions consists of a depletion layer capacitance in parallel with bulk resistance of the device R_1 and a series resistance of contacts R_2. The parameters R_1, R_2, and C were determined from the fitting using a data evaluation software Solartron Z-plot. It was found that, for the quantum dot sample, R_1 decreases from the value of 2×10^{11} Ω at 77 K to 1×10^{6} Ω at 300 K, whereas, R_2 changes only very slightly with temperature. Its value increases from 58 Ω at 77 K to 66 Ω at 300 K. Capacitance increases from 53 pF to 61 pF, respectively. For the reference sample, R_1 decreases from the value of 2×10^{10} Ω at 77 K to 1×10^{6} Ω at 300 K, whereas R_2 increases from the value of 64 Ω at 77 K to 70 Ω at 300 K. As in the case of the QD sample, capacitance also increases, from 68 pF to 73 pF, respectively. In both cases, the resistance R_1 is thermally activated, as it changes with temperature over a few decades. The resistance R_2 can be attributed to the contact resistance of both samples, as mentioned earlier.

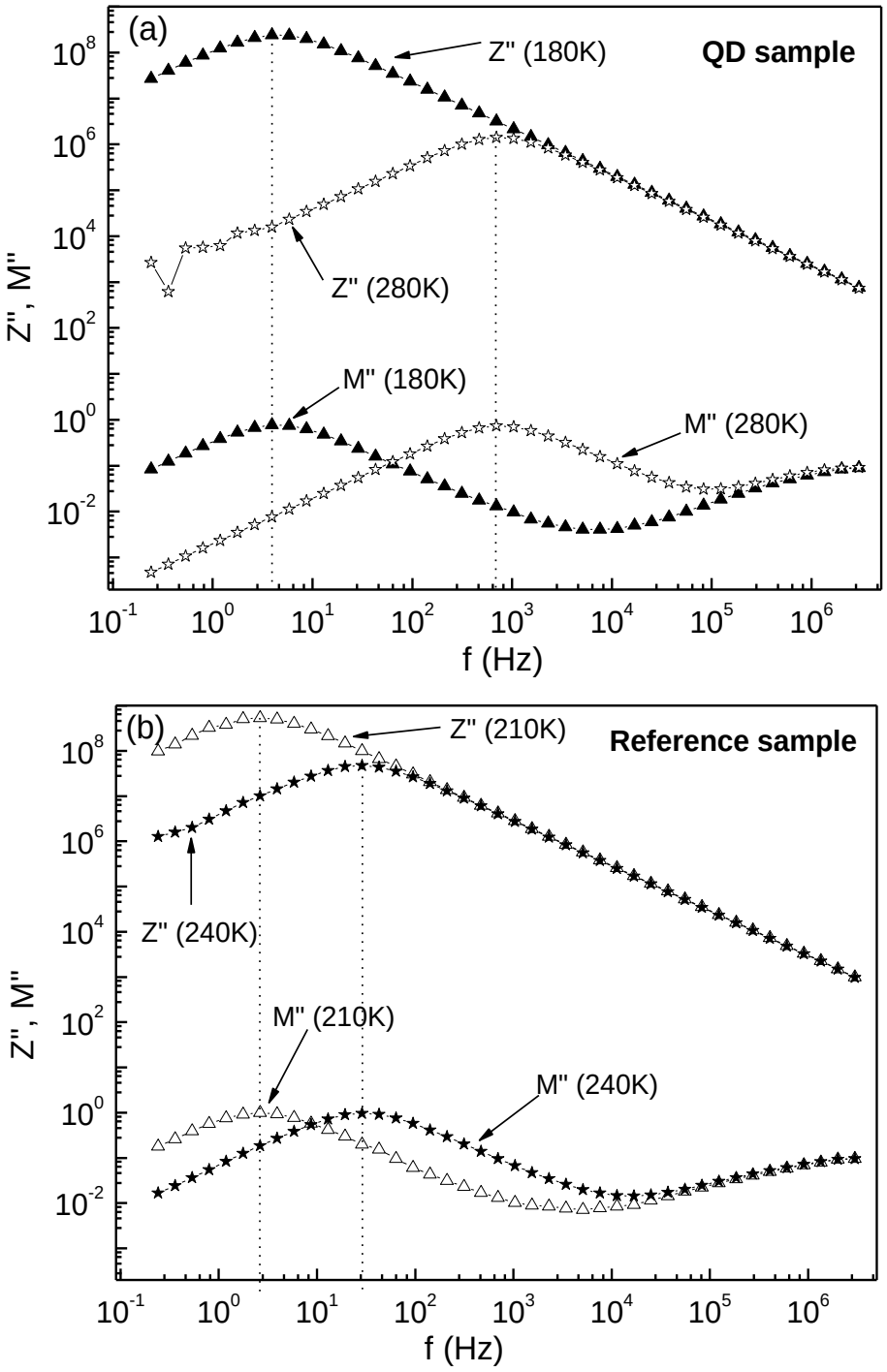


Figure 6. Comparison of plots of the imaginary parts of electric modulus and impedance vs. frequency for the quantum dot (**a**) and reference sample (**b**). For both samples, the maxima correspond to the same frequency.

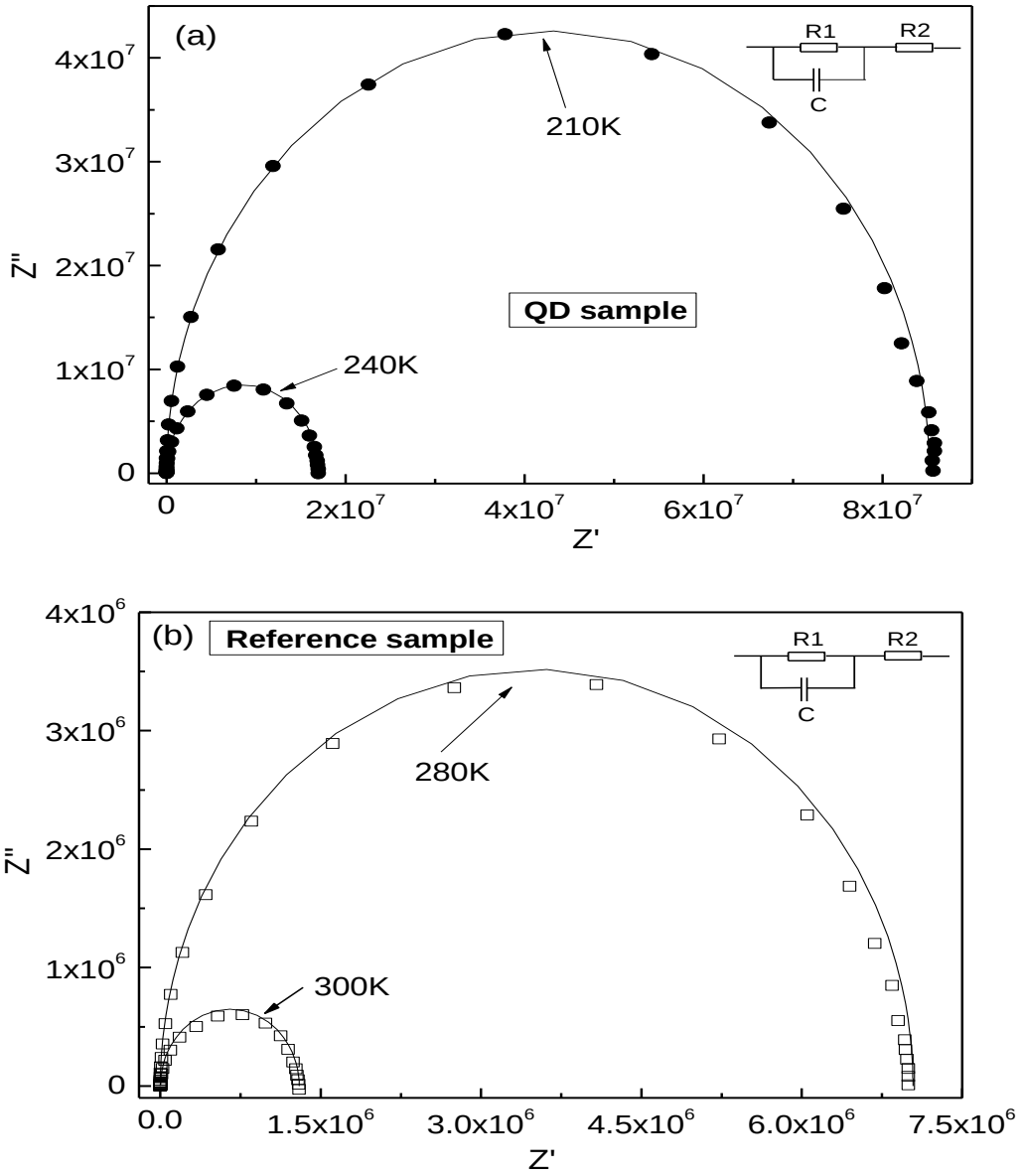


Figure 7. Complex impedance plane plots for the quantum dot (**a**) and reference sample (**b**). Empty squares and full dots—experimental data, solid lines—fitting with the electric circuit shown in the insets.

In Figure 8a, the Arrhenius plots of the relaxation frequency corresponding to the peaks of impedance and electric modulus given in Figure 4a,b and Figure 5a,b for the reference and quantum dot samples are presented. In Figure 8b, the Arrhenius plots of $ln(R_1)$ versus $1/T$ for both samples are shown. The plots reveal a value of the activation energy close to 0.2 eV for the QD sample and ~0.4 eV for the reference sample. The activation energies calculated from the Arrhenius plots of $ln(f_{max})$ versus $1/T$ and $ln(R_1)$ versus $1/T$ are nearly the same; therefore, it can be concluded that the relaxation process may be attributed to the same type of traps present in both junctions.

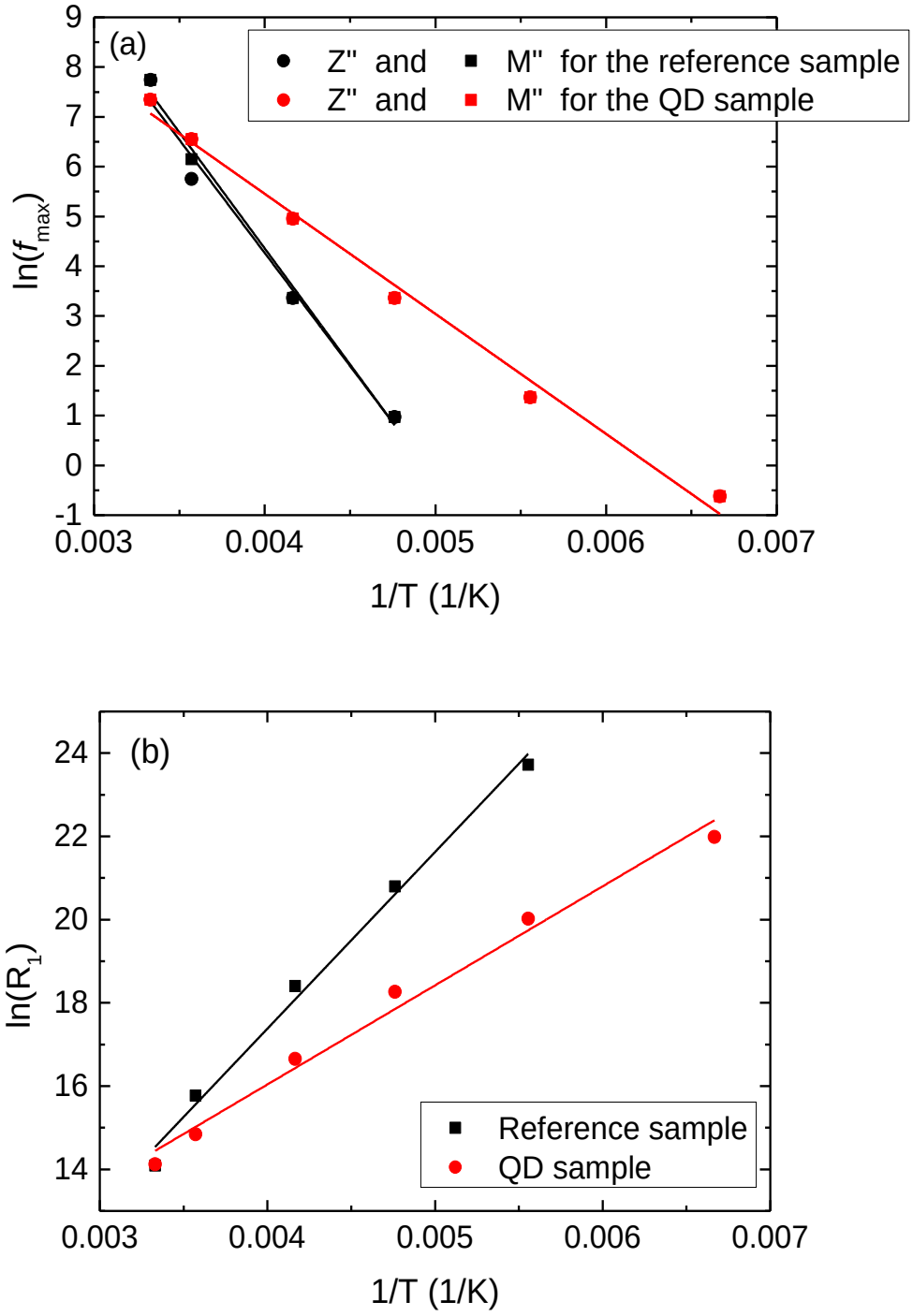


Figure 8. Arrhenius plots of $ln(f_{max})$ vs. $1/T$ (**a**) and $ln(R_1)$ vs. $1/T$ (**b**) for the reference and quantum dot samples.

In the case of the QD sample, the trap of activation energy equal to 0.2 eV is detected. Now, the question is whether the trap is related to the confinement depth of hole levels in CdTe QDs with respect to the valence band edge of *p*-type ZnTe/N or thermal emission of the holes from the trap that accompanies QDs' formation. It is well known that the CdTe–ZnTe valence band offset is in the order of 0.1 eV [25]. Thus, one may expect that the value of the thermal activation energy for emission of holes from CdTe QDs to the respective valence band is close to this value. However, it should be pointed out that, owing to variations in the energy induced by size and strain fluctuations from dot to dot, the energy obtained from the measurements can deviate strongly from the theoretical value.

The 0.2 eV activation energy trap may be connected either with the carrier emission from the QDs themselves to the valence band or with the thermal emission of holes from the traps that accompany QDs' formation. The DLTS measurements performed by us on the same QDs and samples without QDs confirm the presence of the trap of the same thermal activation energy [12]. Thus, we assume that the 0.2 eV level is associated rather with defects that decorate QDs than the direct emission of holes from QD states to the ZnTe valence band. A detailed analysis has been performed in [12]. The growth of QDs is presumably accompanied by the creation of defects of density dominating over the density of defects already present in ZnTe matrix. Therefore, it is also possible that QD growth favours the enhancement of Zn migration, and the observed 0.2 eV trap can be attributed to Zn vacancy occurring in ZnTe [12,26,27]. However, the 0.2 eV trap is not observed for the reference sample. The 0.4 eV level can be assigned to the bulk ZnTe material, as also revealed DLTS studies (cf. [12]).

4. Conclusions

The studies presented in this paper were dedicated to a sample with CdTe self-assembled quantum dots embedded in ZnTe (*p*-type) matrix and a reference structure, without the QDs. Schottky junctions based on the aforementioned samples were realized to perform electrical measurements. *I-V* plots showed the rectifying properties of the diodes and revealed that the presence of CdTe quantum dots in the Ti/Al–ZnTe Schottky junction does not change significantly its electric parameters. The values of barrier heights obtained from *I-V* characteristics for the reference and QD samples are almost the same and are around 0.7 eV. The *C-V* method revealed the net acceptor concentration in the order of 10^{15} cm^{-3} for both samples. Nevertheless, the *C-V* plot for the junction with CdTe QDs exhibits a characteristic step related to the accumulation of carriers in the QD states. This result confirms the presence of quantum dots in the investigated diode. The complex impedance spectroscopy technique was applied to characterize the thermal emission of carriers from defects related to QDs in the studied QD sample. Additionally, an equivalent *RC* circuit model has been proposed for the investigated Schottky junctions to understand their principle of operation and mechanisms of charge transport. It consists of a depletion layer capacitance in parallel with bulk resistance of the device and a series resistance of contacts. The imaginary part of electric modulus and impedance versus frequency plots reveal the presence of relaxation peaks appearing at the same frequency for both samples, whereas the imaginary part of capacitance does not exhibit any relaxation peaks within the measured frequency range. Such behavior along with the high relaxation ratio *r* is indicative for a long-range conductivity type of relaxation. The activation energy of the trap related to the dominant relaxation peak observed for the QD sample obtained from the Arrhenius plot of the resistance, impedance, and modulus equals 0.2 eV. For the reference sample, the value of activation energy determined with the help of the same methods is equal to ~0.4 eV. In conclusion, it was assumed that the 0.4 eV trap is related to ZnTe host material, whereas that observed for the QD sample corresponds to the thermal activation of holes from the defects decorating CdTe QDs.

Author Contributions: Conceptualization, E.Z.; methodology, E.Z.; formal analysis, E.Z.; investigation, E.Z.; resources, G.K.; writing—original draft preparation, E.Z.; writing—review and editing, E.Z. and E.P.-P.; supervision, E.P.-P.; funding acquisition, E.Z., E.P.-P. and G.K. All authors have read and agreed to the published version of the manuscript.

Funding: The research was partially supported by the statutory grant (No. 8201003902) of Department of Quantum Technologies of Wroclaw University of Science and Technology.

Conflicts of Interest: The authors declare no conflict of interest. The funders had no role in the design of the study; in the collection, analyses, or interpretation of data; in the writing of the manuscript, or in the decision to publish the results.

References

1. Barnham, K.; Vvedensky, D. *Low-Dimensional Semiconductor Structures*; Cambridge University Press: Cambridge, UK, 2001; pp. 1–55.

2. Blood, P.; Orton, J.W. *The Electrical Characterization of Semiconductors: Majority Carriers and Electron States*; Academic Press: San Diego, CA, USA, 1992; pp. 596–648.
3. Nauka, K.; Kamins, T.I.; Turner, J.E.; King, C.A.; Hoyt, J.L.; Gibbons, J.F. Admittance spectroscopy measurements of band offsets in $Si/Si_{1-x}Ge_x/Si$ heterostructures. *Appl. Phys. Lett.* **1992**, *60*, 195–197. [CrossRef]
4. Jonscher, A.K. Dielectric relaxation in solids. *J. Phys. D Appl. Phys.* **1999**, *32*, R57–R70. [CrossRef]
5. Bellakhder, H.; Outzourhit, A.; Ameziane, E.L. Study of ZnTe thin films deposited by r.f. sputtering. *Thin Solid Films* **2001**, *382*, 30–33. [CrossRef]
6. Kashyout, A.B.; Arico, A.S.; Antonucci, P.L.; Mohamed, F.A.; Antonucci, V. Influence of annealing temperature on the opto-electronic characteristics of ZnTe electrodeposited semiconductors. *Mater. Chem. Phys.* **1997**, *51*, 130–134. [CrossRef]
7. Bimberg, D.; Grundmann, M.; Ledentsov, N.N. *Quantum Dot Heterostructures*; Wiley: New York, NY, USA, 1999; pp. 1–339.
8. Kazimierczuk, T.; Smolenski, T.; Kobak, J.; Goryca, M.; Pacuski, W.; Golnik, A.; Fronc, K.; Kłopotowski, Ł.; Wojnar, P.; Kossacki, P. Optical study of electron-electron exchange interaction in CdTe/ZnTe quantum dots. *Phys. Rev. B* **2013**, *87*, 195302. [CrossRef]
9. Lee, H.S.; Rastelli, A.; Benyoucef, M.; Ding, F.; Kim, T.W.; Park, H.L.; Schmidt, O.G. Microphotoluminescence spectroscopy of single CdTe/ZnTe quantum dots grown on Si(001) substrates. *Nanotechnology* **2009**, *20*, 075705. [CrossRef]
10. Godo, K.; Makino, H.; Takai, T.; Chang, J.H.; Yao, T.; Sasao, T.; Goto, T. Band Filling and Thermal Escape in CdTe/ZnTe Quantum Dots Grown by Molecular Beam Epitaxy. *Phys. Stat. Sol.* **2002**, *229*, 439–443. [CrossRef]
11. Pautrat, J.L.; Magnea, N.; Faurie, J.P. The segregation of impurities and the self-compensation problem in II-VI compounds. *J. Appl. Phys.* **1982**, *53*, 8668–8677. [CrossRef]
12. Zielony, E.; Placzek-Popko, E.; Nowakowski, P.; Gumienny, Z.; Suchocki, A.; Karczewski, G. Electro-optical characterization of Ti/Au–ZnTe Schottky diodes with CdTe quantum dots. *Mater. Chem. Phys.* **2012**, *134*, 821–828. [CrossRef]
13. Ragunathan, G.; Kobak, J.; Gillard, G.; Pacuski, W.; Sobczak, K.; Borysiuk, J.; Skolnick, M.S.; Chekhovich, E.A. Direct measurement of hyperfine shifts and radio frequency manipulation of nuclear spins in individual CdTe/ZnTe quantum dots. *Phys. Rev. Lett.* **2019**, *122*, 096801. [CrossRef]
14. Jin, S.H.; Choi, J.C.; Lee, H.S. Temperature-dependent photoluminescence in CdTe/ZnTe triple quantum dots. *J. Korean Phys. Soc.* **2019**, *74*, 173–176. [CrossRef]
15. Jin, S.H.; Kim, S.H.; Man, M.T.; Choi, J.C.; Lee, H.S. Thermal escape and carrier dynamics in multilayer CdTe/ZnTe quantum dots. *J. Alloy. Compd.* **2018**, *735*, 2119–2122. [CrossRef]
16. Rouis, W.; Sayari, A.; Nouiri, M.; Ezzdini, M.; Rekaya, S.; El Mir, L.; Sfaxi, L.; Maaref, H. Characterization of the GaAs-based intermediate band solar cellwith multi-stacked InAs/InGaAs quantum dots. *Int. J. Nanotechnol.* **2015**, *12*, 584–596. [CrossRef]
17. Zhao, J.; Liu, Z.; Tang, H.; Jia, C.; Zhao, X.; Xue, F.; Wei, L.; Kong, G.; Wang, C.; Liu, J. Enhanced performance of solar cells via anchoring CuGaS2 quantum dots. *Sci. China Mater.* **2017**, *60*, 829–838. [CrossRef]
18. Khan, J.; Yang, X.; Qiao, K.; Deng, H.; Zhang, J.; Liu, Z.; Ahmad, W.; Zhang, J.; Li, D.; Liu, H.; et al. Low-temperature-processed SnO_2–Cl for efficient PbS quantum-dot solar cells via defect passivation. *J. Mater. Chem. A* **2017**, *5*, 17240–17247. [CrossRef]
19. Jin, Z.; Wang, A.; Zhou, Q.; Wang, Y.; Wang, J. Detecting trap states in planar PbS colloidal quantum dot solar cells. *Sci. Rep.* **2016**, *6*, 37106. [CrossRef]
20. Sze, S.M. *Physics of Semiconductor Devices*, 2nd ed.; Wiley: New York, NY, USA, 1981; pp. 225–234.
21. Brunkov, P.N.; Kovsh, A.R.; Ustinov, V.M.; Musikhin, Y.G.; Ledentsov, N.N.; Konnikov, S.G.; Polimeni, A.; Patanè, A.; Main, P.C.; Eaves, L.; et al. Emission of electrons from the ground and first excited states of self-organized InAs/GaAs quantum dot structures. *J. Electron. Mater.* **1999**, *28*, 486–490. [CrossRef]
22. Gerhardt, R. Impedance and dielectric spectroscopy revisited: Distinguishing localized relaxation from long-range conductivity. *J. Phys. Chem. Solids* **1994**, *55*, 1491–1506. [CrossRef]
23. Lanfredi, S.; Rodrigues, A.C.M. Impedance spectroscopy study of the electrical conductivity and dielectric constant of polycrystalline $LiNbO_3$. *J. Appl. Phys.* **1999**, *86*, 2215–2219. [CrossRef]
24. Barsoukov, E.; Macdonald, J.R. *Impedance Spectroscopy: Theory, Experiment, and Applications*, 3rd ed.; John Wiley & Sons, Inc.: Hoboken, NJ, USA, 2018; pp. 1–292.

25. Continenza, A.; Massidda, S. Electronic properties and valence-band offset of strained ZnTe/CdTe (001) superlattices. *Phys. Rev. B* **1994**, *50*, 11949–11954. [CrossRef]
26. Tubota, H. Electrical Properties of $A^{II}B^{VI}$ Compounds, CdSe and ZnTe. *Jpn. J. Appl. Phys.* **1963**, *2*, 259–265. [CrossRef]
27. Horikoshi, Y.; Ebina, A.; Takahashi, T. Optical Absorption Due to Acceptor Levels in Undoped ZnTe. *Jpn. J. Appl. Phys.* **1972**, *11*, 992–1001. [CrossRef]



© 2020 by the authors. Licensee MDPI, Basel, Switzerland. This article is an open access article distributed under the terms and conditions of the Creative Commons Attribution (CC BY) license (http://creativecommons.org/licenses/by/4.0/).